The role of North Atlantic blocking high during large-scale heavy rainfall events over central India

Akshaya C. Nikumbh,[a,b] A. B. S. Thakur,[c,d] Arindam Chakraborty,[c,d] G.S. Bhat,[c,d] Jai Sukhatme,[c,d]

[a] *Geophysical Fluid Dynamics Laboratory (NOAA), Princeton, New Jersey, 08540, USA.*

[b] *Atmospheric and Oceanic Sciences (AOS), Princeton University, Princeton, New Jersey, 08540, USA.*

[c] *Centre for Atmospheric and Oceanic Sciences, Indian Institute of Science, Bangalore, 560012, India.*

[d] *Divecha Centre for Climate Change, Indian Institute of Science, Bangalore, 560012, India*

Corresponding author: Akshaya C. Nikumbh, Akshaya.Nikumbh@noaa.gov.in

1

ABSTRACT: Large-scale extreme rainfall events (LEREs) over central India are produced by monsoon low-pressure systems (LPSs) when assisted by a secondary cyclonic vortex (SCV). Both the LPS and the SCV are embedded in a monsoon trough and form mainly during the positive phase of the boreal summer intraseasonal oscillation. Here, we observe that tropical-extratropical interactions exist during LEREs. Using ray tracing, we show that extratropical Rossby waves propagate to the Indian subcontinent during the summer monsoon season. Stationary Rossby wave rays originating over the north Atlantic ocean reach India following approximately a great circle path at mid-tropospheric levels. This pathway appears to play an important role in tropical-extratropical interactions during LEREs. 77 % of LEREs are preceded by a north Atlantic blocking high and 90 % by a quasi-stationary central Asian high. The Atlantic blocking high triggers a quasi-stationary Rossby wave response and strengthens the downstream central Asian high. In turn, the quasi-stationary central Asian high facilitates Rossby wave breaking, transporting high PV streamers and cut-offs equatorward. The central Asian high is in close proximity to the monsoon trough in the mid and lower troposphere. It interacts with the monsoon trough over the northwest Indian subcontinent. The equatorial monsoon trough is strengthened due to the supply of dynamic forcing and static instabilities from the extratropics. This additional forcing from the extratropics creates an environment that is conducive for LEREs.

2

1. Introduction

The lateral energy transport between tropics and midlatitudes occurs through various tropical-extratropical interactions in the atmosphere and ocean. These interactions are two-way and occur at time scales ranging from daily to climate, with faster scales in the atmosphere. Theoretical and observational investigation of tropical-extratropical interactions has a long history (Riehl 1950; Bjerknes 1969; Charney 1969; Stan et al. 2017). Charney (1969) suggested that midlatitude disturbances can propagate into the tropics where zonal winds are westerly or weak easterly and mainly at upper levels. Subsequently, several studies confirmed this and showed that extratropical disturbances enter into the tropics mainly in upper level westerly regions (Hoskins et al. 1977; Webster and Holton 1982; Branstator 1983).

Over the Indian subcontinent, extratropical influence on the summer monsoon was noted by Ramaswamy (1958) during the break phase, when below-average rainfall is observed over the core monsoon zone. The focus of most studies in this area has mainly been on examining extratropical disturbances initiating the break phase of the monsoon (Ramaswamy 1962; Raman and Rao 1981; Krishnan et al. 2009; Samanta et al. 2016; Borah et al. 2020). Possibly because the subtropical westerly jet moves southward during the monsoon break, enabling extratropical disturbances to intrude southward. Almost half of the 20th century droughts over India during the summer monsoon are shown to be associated with the mid-latitude Rossby waves (Borah et al. 2020). The monsoon breaks are triggered when the westerly trough shifts southward over northwest India and Pakistan region (Krishnan et al. 2009).

The monsoon flow has a strong easterly jet at upper levels during the active phase and it can inhibit the extratropical intrusion. However, studies have noted the role of extratropical waves in promoting convection even during active monsoon conditions (Kripalani et al. 1997; Ding and Wang 2005, 2007, 2009; Chakraborty and Agrawal 2017; Di Capua et al. 2020). Kripalani et al. (1997) showed that active conditions over north and central India are preceded by a high over northwest India. Ding and Wang (2005) suggested possible two-way interactions between the monsoon and the circumglobal teleconnection pattern. The wave train excited at the exit of the jet stream over the Atlantic can affect the west-central Asian high and thereby enhance convection over the monsoon region by changing the intensity of vertical easterly shear (Ding and Wang 2007). Conversely, the extreme monsoon convection can reinforce the west-central Asian high and trigger

3

the downstream Rossby wave train. Chakraborty and Agrawal (2017) showed that an anomalous surface pressure low over western Asia during the pre-monsoon months can lead to the early onset of monsoon by modulating the low level circulation. Anomalous low pressure over Asia enhances the meridional pressure gradient, which strengthens the low-level jet. The enhanced meridional shear associated with the jet can trigger the onset vortex and thereby favours the early onset.

The above observational and modelling studies suggest that tropical-extratropical interactions exist during both the break and active phases of the monsoon. However, there remains a theoretical disconnect of the possibility of extratropical wave intrusion during the monsoon, given that upper levels have a strong easterly jet during active conditions. In this work, we investigate this aspect by using the Rossby wave ray tracing technique (Karoly 1983). A wave ray is the integral path of the group velocity which shows the propagation of wave energy (Karoly 1983). It is used to assess the remote atmospheric response to a localized forcing (Wang et al. 2007; Zhao et al. 2015; Feng et al. 2017; Rondanelli et al. 2019). The original theory of the Rossby wave propagation using the β-plane approximation on a uniform basic state was extended by Hoskins and Karoly (1981) to incorporate disturbances on a latitudinally varying flow. Karoly (1983) obtained the dispersion relation and equations needed to describe Rossby waves on a fully nonuniform two dimensional flow. Using this complete formulation, Li et al. (2015) demonstrated that Rossby waves can propagate through the pockets of easterlies as well. During the summer monsoon season, the upper-level atmosphere has a strong easterly jet and the mid-to low level monsoon flow is westerly, making it an interesting candidate to understand these developments in the theory of Rossby wave propagation. Using the background conditions of the summer monsoon, where the basic state is horizontally nonuniform, we check if it is possible for the Rossby waves to come over India.

The effect of extratropical forcing on extreme rainfall events during the summer monsoon has started receiving attention in recent decades. Vellore et al. (2016) showed that extreme precipitation events such as the 2013 Uttarakhand floods over the Himalayan region were triggered by the extratropical trough intrusion. Similarly, the role of Rossby waves and teleconnection during heavy rainfall events over Pakistan, northern India, Nepal and Tibet have been well documented (Lau and Kim 2012; Martius et al. 2013; Hunt et al. 2018; Priya et al. 2017; Bohlinger et al. 2017). These studies are confined mainly to the northern latitudes of the Indian subcontinent. However, some case studies have noted the extratropical influence during extreme rainfall events over the

4

southern states of India (Chakraborty 2016; Lyngwa and Nayak 2021). The extratropical influence on extreme rainfall events over central India has not received much attention except for a few studies (Nikumbh et al. 2019; Sooraj et al. 2020). Nikumbh et al. (2019) noted that low pressure systems producing large-scale extreme rainfall events (LEREs, $area \geq 70,000 km^2$) are assisted by planetary-scale circulation but did not examine its influence. Sooraj et al. (2020) examined the role of surface thermal forcing and moist processes over northwest India in triggering heavy rainfall events over central India.

Nikumbh et al. (2020) showed that LEREs are triggered when monsoon low-pressure systems are assisted by a secondary cyclonic vortex (SCV) to its west. The presence of multiple synoptic systems is observed usually during the active (positive) phase of boreal summer intraseasonal oscillations when a monsoon trough is present over the core monsoon zone. Consequently, Nikumbh et al. (2021) observed that LEREs over central India occur mainly during the positive phase of boreal summer intraseasonal oscillations. The influence of extratropical circulation during LEREs remains to be investigated. The main objective of this work is to understand tropical-extratropical interactions during LEREs over central India.

The next section details the data and methodology. We check if extratropical Rossby waves can come over the Indian subcontinent during the summer monsoon in section 3a. Then, we examine meteorological conditions during LEREs in section 3b and study processes in section 3c. A summary and discussion are given in section 4.

2. Methods

We use the daily $1° \times 1°$ rainfall data from India's meteorological department (Rajeevan et al. 2006) and define extreme rainfall by using the 99.5^{th} percentile. Following Nikumbh et al. (2019), LEREs are detected using the connected component algorithm (Falcão et al. 2004) that can identify the neighbouring grids that receive extreme rainfall simultaneously. LEREs occupy more than five $1° \times 1°$ neighbouring grids ($area \geq 70 \times 10^3 km^2$). We examine LEREs over central India (15°-25°N, 65°–85° E) for the period 1979 to 2012. A total of 22 LEREs were observed during the study period. More details on the identification of LEREs can be found in Nikumbh et al. (2019) and Nikumbh et al. (2020). The daily ERA-Interim dataset (Dee et al. 2011) at the horizontal

5

resolution of $1° \times 1°$ is used for the analysis. Day(0) indicates the day of LEREs and composite anomalies are calculated by subtracting the daily climatology.

a. Rossby ray tracing

We trace Rossby wave trajectories following Karoly (1983) and Li et al. (2015). We look for wave-like solutions to the non-divergent barotropic vorticity equation linearized about two dimensionally varying climatological background flow. This yields the following dispersion relation:

$$\omega = \overline{u}_M k + \overline{v}_M l + \frac{l \partial_x \overline{q} - k \partial_y \overline{q}}{k^2 + l^2} \tag{1}$$

Here, ω is the angular frequency, k and l are the zonal and meridional wavenumbers, $\overline{q}$ is the climatological absolute vorticity, and $\overline{u}_M$ and $\overline{v}_M$ are the climatological zonal and meridional wind, respectively.

The main assumptions in this formulation are a slowly varying background state and the absence of dissipation. The first assumption stems from the requirement that the length scales of the perturbations should be much smaller than those for the background flow (Karoly 1983). This is realized by truncating a two-dimensional Fourier transform of the background flow at the zonal and meridional wavenumber 5 (Li et al. 2015). The second assumption is justified through a further assumption of a stationary wave ($\omega = 0$, $c_p = 0$). This implies that the effects of dissipation are counteracted by energy propagation from the source at the Rossby wave group velocity (Freitas and Rao 2014).

From the dispersion relation (Equation 1), the zonal and meridional components of the group velocity can be obtained as

$$u_g = \partial_k \omega = \overline{u}_M + \frac{(k^2 - l^2) \partial_y \overline{q} - 2kl \partial_x \overline{q}}{(k^2 + l^2)^2} \tag{2}$$

$$v_g = \partial_l \omega = \overline{v}_M + \frac{(k^2 - l^2) \partial_x \overline{q} + 2kl \partial_y \overline{q}}{(k^2 + l^2)^2} \tag{3}$$

Given the two-dimensional variation of the flow, both k and l may change along the ray path. Their evolution can be captured by the following relations (Karoly 1983; Li et al. 2015)

6

Accepted for publication in *Journal of the Atmospheric Sciences*. DOI 10.1175/JAS-D-22-0185.1.

resolution of $1° \times 1°$ is used for the analysis. Day(0) indicates the day of LEREs and composite anomalies are calculated by subtracting the daily climatology.

a. Rossby ray tracing

We trace Rossby wave trajectories following Karoly (1983) and Li et al. (2015). We look for wave-like solutions to the non-divergent barotropic vorticity equation linearized about two dimensionally varying climatological background flow. This yields the following dispersion relation:

$$\omega = \overline{u}_M k + \overline{v}_M l + \frac{l \partial_x \overline{q} - k \partial_y \overline{q}}{k^2 + l^2} \tag{1}$$

Here, ω is the angular frequency, k and l are the zonal and meridional wavenumbers, $\overline{q}$ is the climatological absolute vorticity, and $\overline{u}_M$ and $\overline{v}_M$ are the climatological zonal and meridional wind, respectively.

The main assumptions in this formulation are a slowly varying background state and the absence of dissipation. The first assumption stems from the requirement that the length scales of the perturbations should be much smaller than those for the background flow (Karoly 1983). This is realized by truncating a two-dimensional Fourier transform of the background flow at the zonal and meridional wavenumber 5 (Li et al. 2015). The second assumption is justified through a further assumption of a stationary wave ($\omega = 0$, $c_p = 0$). This implies that the effects of dissipation are counteracted by energy propagation from the source at the Rossby wave group velocity (Freitas and Rao 2014).

From the dispersion relation (Equation 1), the zonal and meridional components of the group velocity can be obtained as

$$u_g = \partial_k \omega = \overline{u}_M + \frac{(k^2 - l^2) \partial_y \overline{q} - 2kl \partial_x \overline{q}}{(k^2 + l^2)^2} \tag{2}$$

$$v_g = \partial_l \omega = \overline{v}_M + \frac{(k^2 - l^2) \partial_x \overline{q} + 2kl \partial_y \overline{q}}{(k^2 + l^2)^2} \tag{3}$$

Given the two-dimensional variation of the flow, both k and l may change along the ray path. Their evolution can be captured by the following relations (Karoly 1983; Li et al. 2015)

Accepted for publication in *Journal of the Atmospheric Sciences*. DOI 10.1175/JAS-D-22-0185.1.

$$\frac{d_g k}{dt} = -\partial_x \omega = -k\partial_x \overline{u}_M - l\partial_x \overline{v}_M - \frac{l\partial_{xx}\overline{q} - k\partial_{yx}\overline{q}}{k^2 + l^2} \tag{4}$$

$$\frac{d_g l}{dt} = -\partial_y \omega = -k\partial_y \overline{u}_M - l\partial_y \overline{v}_M - \frac{l\partial_{xy}\overline{q} - k\partial_{yy}\overline{q}}{k^2 + l^2} \tag{5}$$

where

$$\frac{d_g}{dt} = \partial_t + \vec{c}_g \cdot \nabla$$

is the material derivative moving with the group velocity.

For a given background flow, forcing location, and an initial zonal wavenumber, the initial meridional wavenumber can be obtained from Equation 1. We retain only the real roots of the cubic equation. The system of equations 2, 3, 4, and 5 are solved using Runge Kutta 4th order method. The time-step is chosen to be 10 minutes and the integration time is 20 days. The integration was terminated if the total wavenumber exceeded 40. In this study, the rays were initiated at forcing sites all over the north Atlantic ($0 - 70°$N, $10 - 70°$W), and with zonal wave numbers $k = 3 - 8$. The Rossby rays were then traced for smoothed climatological flows of June, July, August and September.

b. Identification of north Atlantic blocking high (ABH), Central Asian high (CAH) and high potential vorticity (PV) intrusion

We identify atmospheric blocking high over the Euro-Atlantic region ($10° - 80°$N, $70°W - 10°E$) by using geopotential height anomalies at 500 hPa, following Steinfeld, D., 2020: ConTrack - Contour Tracking algorithm. The code is publicly available via GitHub (`https://github.com/steidani/ConTrack`). The individual blocks are identified when geopotential height anomalies exceed the threshold of the 95th percentile and persist for at least two days with a minimum 50 % spatial overlap between the consecutive anomalies. The anomalies are calculated with respect to the calendar-month averages over the ERA-Interim reanalysis period 1979–2018. For LEREs, we check if the blocking high was present over the Euro-Atlantic region (referred to as ABH in this study) from ten days before the event (day(-10)) to the event day (day(0)).

We identify the location of a high over central Asia (referred to as CAH in this study) and the associated PV intrusion subjectively to indicate the features that would help in triggering

7

LEREs. The CAH is detected when the geopotential height anomalies exceed 30 m from the daily climatology over the region (30°-60°N, 40°-90°E) from five days before the event (day(-5)) to the event day (day(0)). Figure 2 and Supplementary Figure (2-22) indicate the location of CAH and associated PV intrusion. As noted by Postel and Hitchman (1999), the daily maps show a large variation in the location of this subtropical high and the associated PV intrusion. The climatological 2 PVU contour stays north of 30°N during the boreal summer and the standard deviation over the Indian subcontinent is below 0.5 PVU (Supplementary Figure 23). So, we consider the PV intrusion with magnitude of ≥ 0.5 PVU for these events.

c. Wave activity flux

To check the influence of extratropical forcing, we check the wave activity flux proposed by Takaya and Nakamura (2001). The advantage of using the wave activity flux is that it follows a conservation relation under adiabatic and frictionless conditions,

$$\frac{\partial M}{\partial t} + \nabla \cdot W = 0 \tag{6}$$

where M is the density of wave activity and $\nabla \cdot W$ is the associated flux. In slowly varying background conditions (Wentzel–Kramers–Brillouin (WKB) assumption), wave activity flux propagates parallel to the local group velocity (Vanneste and Shepherd 1998; Takaya and Nakamura 2001). The divergence and convergence of W indicate the source and sink of the wave packet, respectively. As the formulation of the wave activity flux by Takaya and Nakamura (2001) is phase-independent, it is suitable to represent phase-averaged statistics. We use the same notation as Takaya and Nakamura (2001) and refer to W as the wave activity flux.

The horizontal wave activity flux (W) is given by,

$$W = C_U M + W_s \tag{7}$$

$$W_s = \frac{p}{2|\mathbf{U}|} \begin{bmatrix} U(\psi_x'^2 - \psi'\psi_{xx}') + V(\psi_x'\psi_y' - \psi'\psi_{xy}') \\ U(\psi_x'\psi_y' - \psi'\psi_{xy}') + V(\psi_y'^2 - \psi'\psi_{yy}') \end{bmatrix} \tag{8}$$

8

where C_U is the phase speed of the wave along the background flow and M indicates wave activity. Hence, the effects of the phase propagation appear only in the term $C_U M$. W_s is a stationary wave activity flux. p, $\mathbf{U} = Ui + Vj$, ψ' are pressure, background wind and quasi-geostrophic perturbation stream function. Here, we calculate stationary wave activity flux (W_s). We use the daily climatological wind for the background flow ($\mathbf{U}$) and apply 11 days moving average while calculating the perturbed quasi-geostrophic stream function. This process removes high-frequency transients.

3. Results

a. Rossby ray path during the summer monsoon

As we are interested in examining LEREs over India, we consider only those rays that can come over the Indian subcontinent from the upstream Atlantic ocean. Fig. 1 indicates that stationary Rossby waves generated in subtropical Atlantic ocean can propagate towards India at midlevels following the great circle path during all four monsoon months. However, each month has slightly different path due to variations in the climatological background flow. During July and August, which are peak monsoon months and have somewhat alike background winds, rays follow similar paths (Fig. 1 b, c). These rays, originating over the subtropical Atlantic ocean (between 20° to 30° W) reach the north Atlantic and Europe in about a week. Then they recurve southward and reach central Asia in about another week of integration time and arch towards northwest India. In June and Septermber, which are the onset and retreat months of the monsoon respectively, the rays originating over the west Africa coast and the west Atlantic ocean can come over the monsoon region (Fig. 1 a, d). In all four months, when ray paths recurve towards India, we can see that they are guided by northerly (southward) and westerly winds. In the upper atmosphere, however, rays follow different trajectories (Supplementary Fig. 1). These rays are reflected poleward near 20° E to 40° E in an area of southerly winds and then continue to follow the westerly jet path. During July and August, rays can come over India by recurving between 100° E to 120° E, near the eastern edge of the Tibetan anticyclone. The upper level rays follow a longer route compared to midlevels and take approximately two weeks to reach over India.
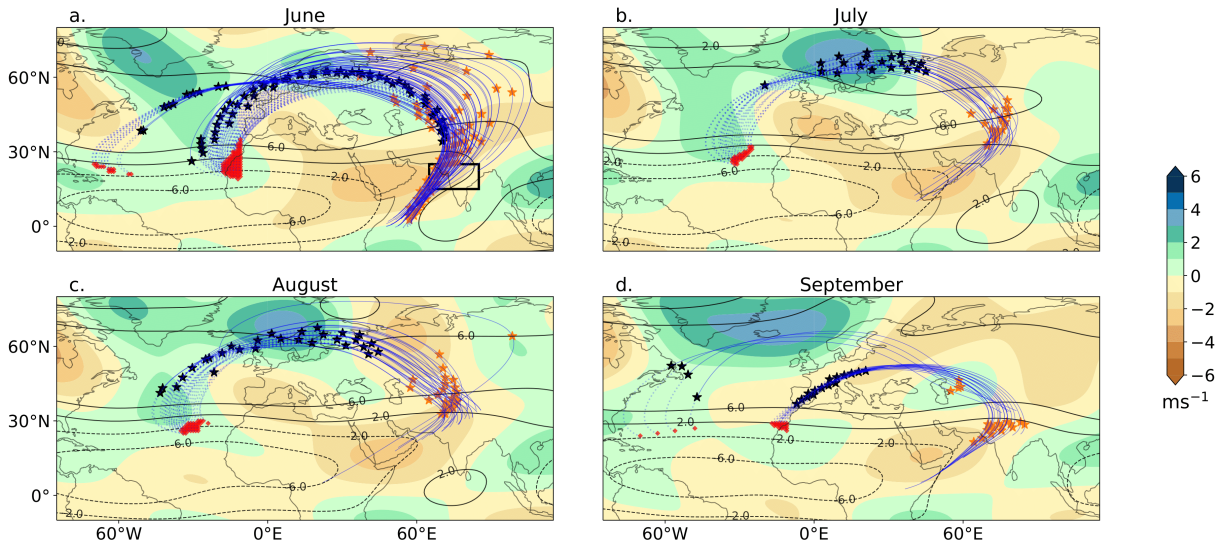
FIG. 1. Rossby wave ray paths at 500 hPa for rays starting with initial zonal wavenumber $k = 4$ during the boreal summer monsoon months. Red markers indicate the starting point (forcing location) for a given ray. The ray path till day 7 is shown as a dotted (blue) line and the rest is a solid line. Black (orange) markers indicate the position at day 7 (14) of integration. The contours indicate the monthly climatological zonal wind and the color shading indicates the same for meridional wind. The monthly climatology shown here is used for the computation of the Rossby ray path. Only those trajectories are shown for which the Rossby rays come over the Indian subcontinent ($10 - 35°$N, $70 - 100°$E). The black inset box indicates the study region ($15 - 25°$N, $65 - 85°$ E).

This analysis suggests that Rossby waves originating over the Atlantic ocean can come over the Indian subcontinent during the summer monsoon months. Rossby waves at midlevel can penetrate over northwest India by recurving near 60° E to 80° E following approximately a great circle path.

b. A quasi-stationary blocking high and wave breaking during LEREs

In this section, we look at the role of the extratropical Rossby wave intrusion during LEREs over central India. The equatorward transport of an extratropical air mass during the breaking of Rossby waves is often observed in the form of PV streamers. The extratropical stratospheric air mass has higher PV (≥ 1.5 PVU, where 1 PVU $= 10^{-6} Km^2 kg^{-1} s^{-1}$) than the tropical air masses (Hoskins et al. 1985). Usually, 2 PVU (or 1.5 PVU) surface is considered as a dynamic tropopause (Hoskins and Berrisford 1988; Hoskins 1997; De Vries et al. 2018; Wernli and Sprenger 2007). PV

10
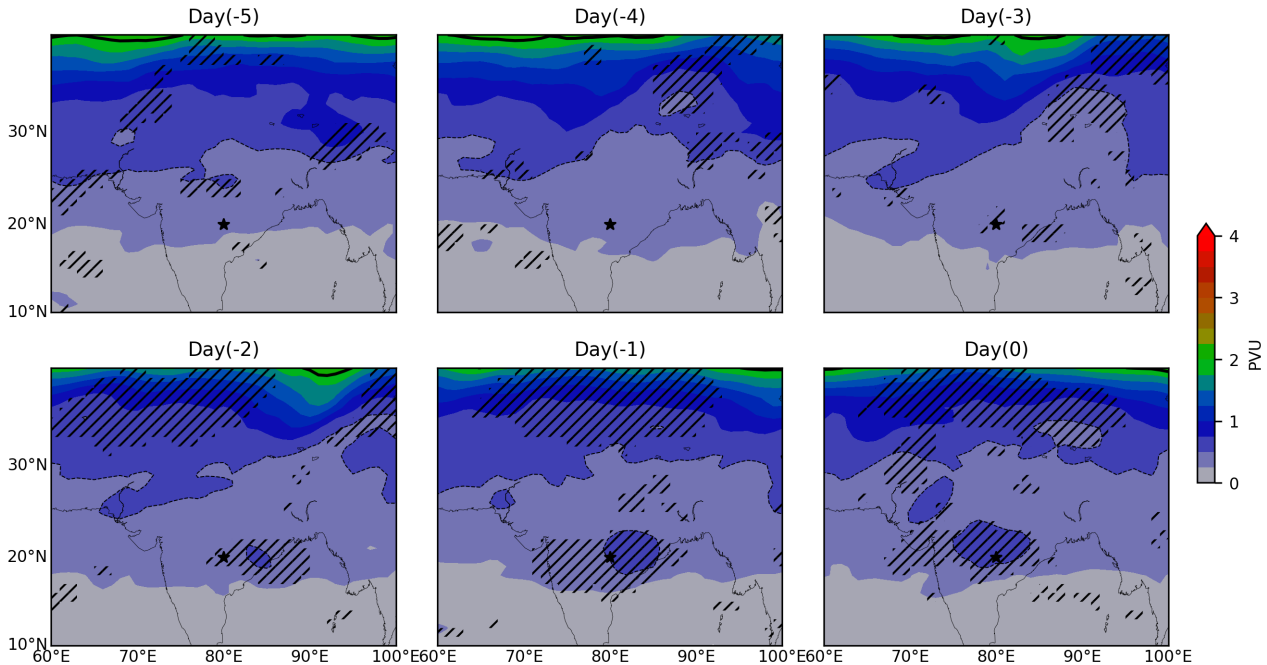
Fig. 2. LERE centric composite potential vorticity at 350 K. The star (20°N, 80°E) indicates the recentered location of LEREs. The daily PV values are remapped with respect to this location for all LEREs. The dotted line indicates a 0.5 PVU contour at the 350 K isentropic level. The hatching represents statistically significant anomalies (t-test: at a 90% significance level). Please note that the map is shown here to get a better idea about an approximate geographical location of PV intrusion for an event that occurs near the reference location. The latitude and longitude values should be interpreted as relative locations with respect to a reference point of 20°N, 80°E.

streamers and the Rossby wave breaking are identified by tracking 2 PVU contours on isentropic surfaces. Supplementray Figures 2-23 show the high PV intrusion for individual events from five days (day(-5)) before the event till the event day (day(0)). We observe that all LEREs are preceded by high PV (PV ≥ 0.5 PVU on 350 K isentropic surface) intrusion (Supplementary Fig. 2-23). However, the location of PV intrusion vary depending upon the location of LEREs. These PV streamers are observed mainly over northwest India. In some cases, we observe that PV cut offs travel westward towards the Indian subcontinent originating from east Asia. Fig. 2 shows LERE-centric composite PV for all events to account for variations in the location of LEREs. The recentered location of LEREs (20°N, 80°E) is roughly close to where the maximum number of

11
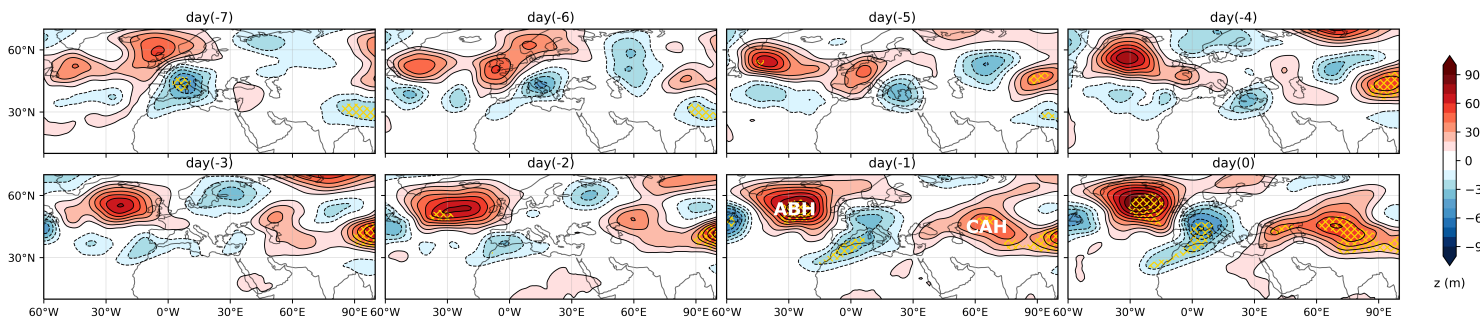
FIG. 3. Lagged composites of anomalous geopotential height at 200 hPa from seven days before the event (day(-7)) to the event day (day(0)) for LEREs. The hatching represents statistically significant anomalies for geopotential height (t-test: $pvalue \leq 0.05$). ABH and CAH indicate the location of the Atlantic Blocking high and Central Asian high, respectively.

LEREs occur (Figure 1b of Nikumbh et al. (2020)). A high PV blob travelling east to west from two days before the event captures the LPS signal. The equatorward high PV intrusion (≥ 0.5 PVU) is seen to the west of LEREs about two to four days before the events. A number of studies have investigated the relationship between the PV intrusion and deep convection triggered on the eastern edges of these intrusions (Kiladis and Weickmann 1992; Kiladis 1998; Waugh and Polvani 2000; Waugh and Funatsu 2003; Knippertz 2007). PV streamers induce vertical motion and static instability on their eastern edge, making the environment conducive for deep convection (Hoskins et al. 1985; Funatsu and Waugh 2008).

To understand the equatorward PV intrusion further, we look at the composite fields for all LEREs. The composite daily evolution of the upper level geopotential height anomalies is shown in Fig. 3. About a week before, a negatively tilted (Northwest-southeast) couplet of a high and a low forms over the eastern Atlantic and western Europe, stretching till north Africa. A weak low and high exist over Asia, downstream of this couplet. Over next two days, a low over central Asia strengthens, stretches meridionally and then moves eastward. On day (-4), a weak high develops over central Asia that moves southward slightly. Then, it remains almost stationary and continues to intensify till the event day. Likewise, ABH remains almost stationary and intensifies. A day before the event, a well-developed wave pattern can be seen that strengthens further on the event day. The locations of the ABH and CAH are somewhat similar to that observed by Ding and Wang (2007) during active monsoon convection over northwest India and Pakistan. The ABH is well investigated
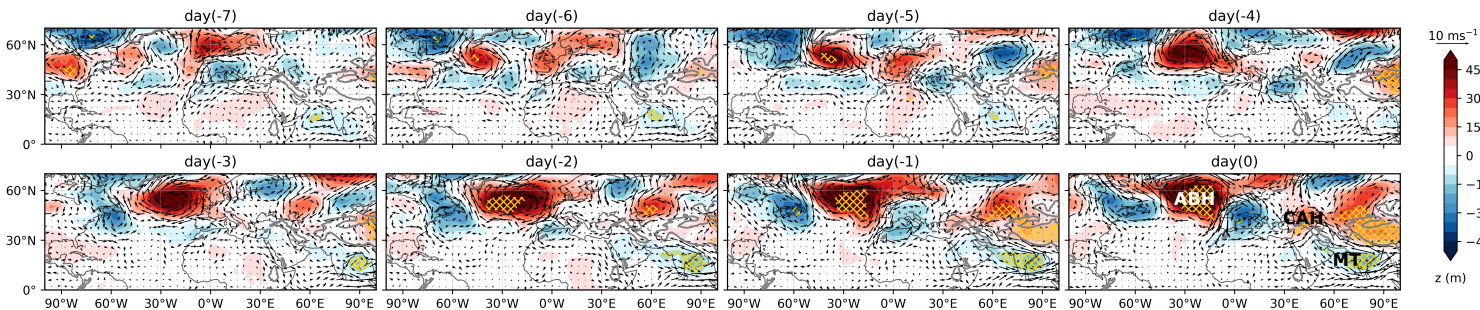
12

F_IG_. 4. Lagged composites of anomalous geopotential height at 500 hPa from seven days before the event (day(-7)) to the event day (day(0)) for LEREs. Vectors indicate the composite of daily anomalous wind. The hatching represents statistically significant anomalies for geopotential height (t-test: $pvalue \leq 0.05$). The gray contours indicate the orography ≥ 1500 m. ABH, CAH, and MT indicate the location of the Atlantic Blocking high and Central Asian high, and monsoon trough, respectively.

feature in the literature (Sanders 1953; Vautard 1990; Cheng and Wallace 1993; Kimoto and Ghil 1993; Woollings et al. 2008). It frequently occurs at the Atlantic strom track exit region (Pelly and Hoskins 2003; Barriopedro et al. 2006; Nakamura and Huang 2018). It is maintained by eddies propagating into a split jet (Shutts 1983; Trenberth 1986; Haines and Marshall 1987; Nakamura et al. 1997), the land-sea contrast (Narinesingh et al. 2020) and modulated by tropical convection (Sardeshmukh 1987; Henderson et al. 2016). We observe that a couplet of Atlantic high and low is indeed accompanied by the split jet (Supplementary Fig. 25). Using a blocking index defined in Section 2, we find that 17 out of 22 LEREs had a presence of ABH (Table S1). On PV-theta surface, a quasi-stationary high can be viewed as a wave breaking event which transfers high PV air equatorward and low PV poleward (Pelly and Hoskins 2003). In the next section, we show that the equatorward high PV transport during LEREs is facilitated by a quasi-stationary CAH.

At midlevels, the similar evolution is observed in the extratropics as at the upper level (Fig. 4). In addition, tropical features are observed over the Indian landmass and nearby ocean. Lows over the Arabian sea and the Bay of Bengal indicate active monsoon conditions. On day(-2), a LPS and an SCV can be seen over the east and west coast of India, respectively (for a close-up view please check Figure 2a of Nikumbh et al. (2020)). An equatorial monsoon trough with the embedded LPS is observed since three days before the event. The equatorial monsoon trough continues to intensify and comes in phase with CAH. The enhanced meridional pressure gradient due to this in-phase
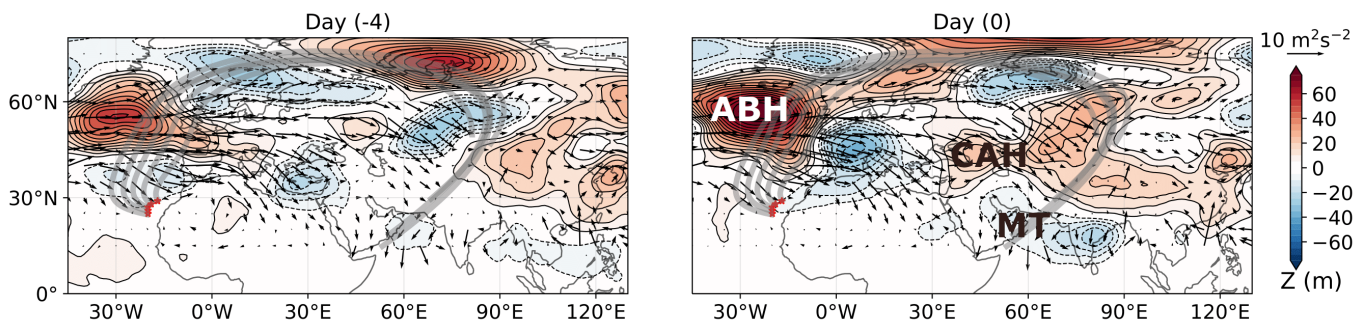
13

Fig. 5. Vectors show the composite wave activity flux for all LEREs calculated using Equation 8 at 500 hPa. The composite geopotential height anomalies at the same level is shown using the shading. The grey paths indicate the Rossby ray paths calculated using the JJAS wind climatology. The features shown using the text are same as shown in Fig. 4.

equatorial trough and CAH strengthens the easterlies on the northern branch of the trough, thereby intensify the equatorial trough. In the following section, we check how extratropical forcing can strengthen the equatorial monsoon trough using wave activity flux, dynamic forcing and static instabilities.

c. Strengthening of the equatorial monsoon trough

1) WAVE ACTIVITY FLUX

The wave activity flux at upper levels shows the eastward and southeastward energy transport from ABH (Supplementary Fig. 26). The strong divergence of wave activity flux in the eastern sector of ABH (Supplementary Fig. 27) indicate the energy transfer to downstream disturbances, which can trigger an anomalous Rossby wave train (Kosaka et al. 2012). Consequently, we see a well established Rossby wave pattern a day before LEREs (Fig. 3). The wave activity converges in between CAH and the Tibetan orography, indicating the wave breaking (Supplementary Fig. 27). The maximum convergence in wave activity flux is observed four days before LEREs. We see the equatorward PV intrusion during LEREs start about 2 to 5 days before the event (Figure 2 and Supplementary Fig. 2-23). Anticyclonic circulation associated with CAH facilitates the transport of high PV air equatorward on its eastern edge. Consequently, we see PV streamers on the eastern edge of CAH (Supplementary Fig. 2-23). We observe that except for two cases (marked as PV, Supplementary Fig.9 and Supplementary Fig. 17), the equatorward PV intrusion is associated with

CAH (Table S1). In section b, we showed that wave breaking is observed during LEREs. Here, we see that the presence of CAH facilitates the wave breaking, thereby transfer high PV airmass equatorward during LEREs.

At midlevels, the wave activity flux emanating from ABH appears to split into two branches (Fig. 5). One approximately along the Rossby ray path calculated from the JJAS wind climatology and the other in a southeastward direction. Near 60° E, the wave activity flux is southerly reaching almost 10° N. On day (0), we see alternate troughs and ridges along the approximately great circle path indicated by Rossby rays. Both CAH and the western branch of the monsoon trough are strengthened along this path. Further, both branches of wave activity flux converge near the location of CAH on the event day. The convergence of wave activity flux indicates the extraction of westerly momentum from the background flow. In other words, the easterly flow is strengthened at the location where we observe the convergence of wave activity flux. Hence, the convergence of wave activity flux facilitated by CAH strengthens the northern branch of the equatorial monsoon trough, which has an easterly flow. As the mid-tropospheric equatorial trough starts developing (Fig. 4), this additional supply of the easterly momentum from the extratropics strengthens it. Especially, since three days before the events, CAH and the equatorial trough come in close proximity and the equatorial monsoon trough intensifies till the event day.

2) Dynamic forcing

Dynamic uplift during LEREs can be checked using the Q-vector (Hoskins et al. 1978). We use the modified form of the Q-vector for the tropics (Kiladis et al. 2006) :

$$\frac{p}{R}\nabla \cdot Q \simeq \frac{\partial T}{\partial x}\frac{\partial \zeta}{\partial y} - \frac{\partial T}{\partial y}\frac{\partial \zeta}{\partial x} - \frac{\partial^2 T}{\partial x \partial y}\left(\frac{\partial^2 \psi}{\partial^2 x} - \frac{\partial^2 \psi}{\partial^2 y}\right) + \frac{\partial^2 \psi}{\partial x \partial y}\left(\frac{\partial^2 T}{\partial^2 x} - \frac{\partial^2 T}{\partial^2 y}\right) \tag{9}$$

where p, R, T, ζ, ψ are pressure, the gas constant for dry air, temperature, the vertical component of relative vorticity, and the stream-function of the horizontal wind, respectively, and other terms have their usual meaning. We plot LERE-centric anomalies of divergence of Q-vector ($|-2\nabla \cdot Q|$) at 600 hPa (Please refer to the caption of Figure 6 for more details). As this field is inherently noisy, we take an average over two areas of interest. The first box is selected at the boundary between CAH and the western branch of the monsoon trough, and the second box is selected around the geometric center of LEREs. On day (-3), we see a weak dynamic uplift between CAH and the
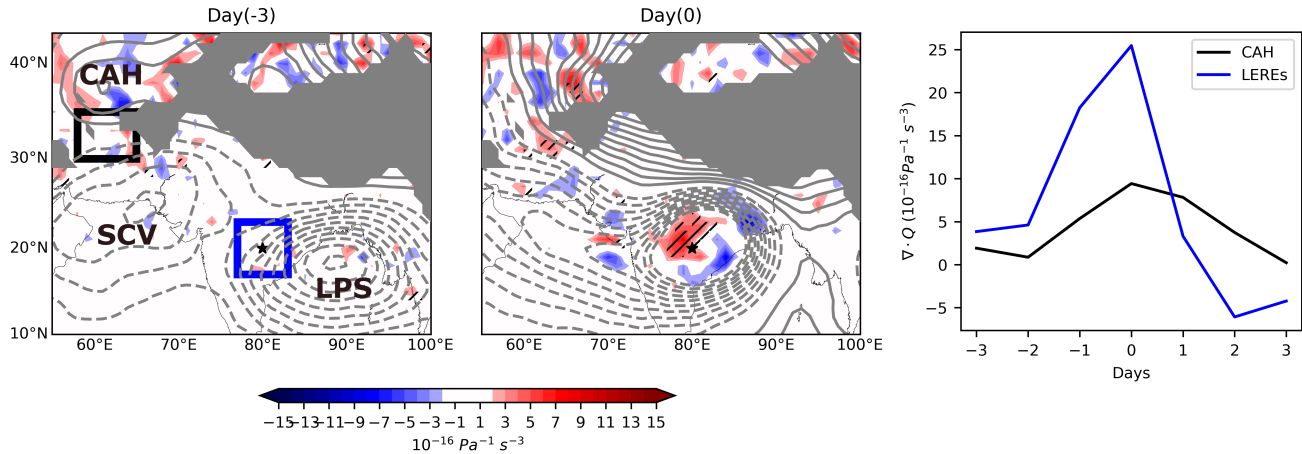
15

FIG. 6.   LERE-centric composite anomalies of divergence of Q-vector ($|-2\nabla \cdot Q|$) (shading) at 600 hPa are shown for day (-3) and day (0) in the left and middle panels, respectively. The star (20° N, 80° E) indicates the recentered location of LEREs. The anomalies are remapped with respect to this location for all LEREs. The contours show composite geopotential height anomalies at 500 hPa. The right panel shows the temporal evolution of dynamic uplift ($|-2\nabla \cdot Q|$) averaged over area shown by a black and a blue box. The blue box shows $5° \times 5°$ latitude-longitude box around the geometric center of LEREs. $4° \times 6°$ black box is selected at the boundary between CAH and monsoon trough. The hatching represents significant anomalies (t-test: $p-value < 0.05$). The location of the Central Asian high (CAH), Secondary cyclonic Vortex (SCV) and monsoon-low pressure system (LPS) are shown using the text. Please note that the map is shown here to get a better idea about features such as an approximate geographical locations of CAH, SCV and LPS , and the locations of dynamic forcing for an event that occurs near the reference location. The latitude and longitude values should be interpreted as relative locations with respect to a reference point of 20°N, 80°E.

western edge of the monsoon trough that has SCV embedded in it. Similarly, we see a weak uplift near LEREs, which is on the western sector of monsoon LPS. The dynamic uplift increases rapidly since two days before the event. As noted by Nikumbh et al. (2020), the circulations associated with SCV and LPS merge at mid-levels a day before the event (their Figure 2a). The strengthened CAH and the monsoon trough lead to enhanced dynamic uplift, which peaks on the event day. On day (0), an alternate enhanced and suppressed dynamic lifting is observed along the northern branch of the monsoon trough, where it interacts with CAH. A large-scale dynamic uplift is seen
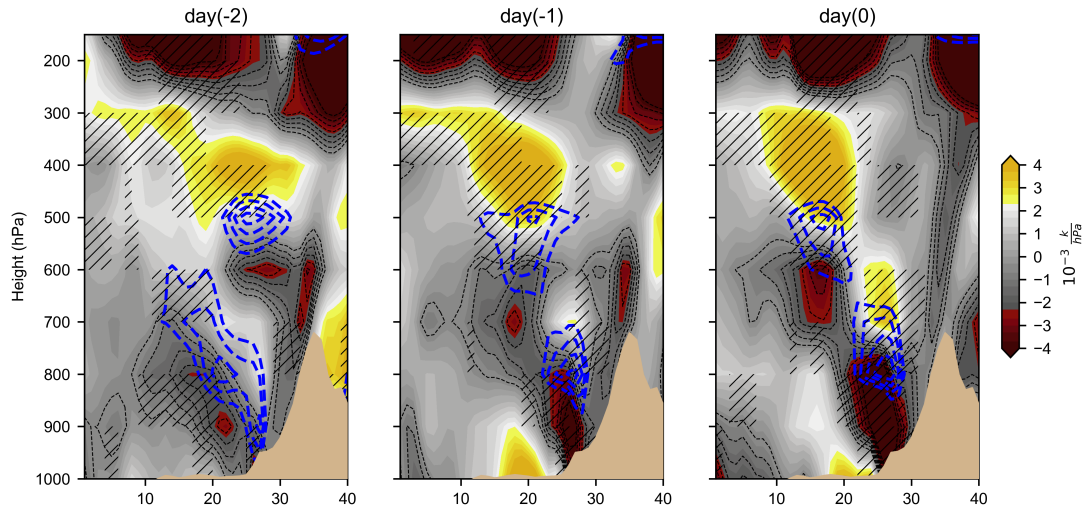
16

FIG. 7. Lagged composite of static stability ($S = \frac{-T}{\theta} \frac{d\theta}{dp}$) anomalies for LEREs from the lag day(-2) to day(0) is shown using the shading. The dotted black contours indicate the negative anomalies (static instabilities) starting from $-0.5 \times 10^{-3} \frac{K}{hPa}$ with a contour interval of $-0.5 \times 10^{-3} \frac{K}{hPa}$. The anomalies are averaged between 60° E to 70° E. The hatching represents statistically significant anomalies (t-test: $p-value < 0.05$). The dotted blue contours represent the composite temperature anomalies starting from -0.2 K with a contour interval of -0.1 K. The orography is shaded in tan color.

at the location of LEREs. Both extratropical and tropical dynamic forcings merge on the event day and trigger LEREs.

3) STATIC STABILITY

The southward intrusion of CAH can bring cold air into the monsoon region. The equatorward cold air surges are known to trigger deep convection over east Asia (Chen et al. 2002, 2012; Park et al. 2014). However, the extratropical cold air intrusion during the Indian summer monsoon has been suggested to be associated mainly with the suppression of convection over central India (Ramaswamy 1962; Raman and Rao 1981; Krishnan et al. 2009; Samanta et al. 2016). These hypotheses are for longer time scales (intra-seasonal to seasonal) and generally use the land-sea contrast agrument. Hence, it is important to examine how cold air advection during extratropical intrusion could affect static stability of atmosphere during LEREs.

17

To understand the possible role of cold air intrusion on convection, we check dry static stability ($S = \frac{-T}{\theta}\frac{d\theta}{dp}$, (Bluestein 1992)). Vertical cross section for temperature anomalies averaged between $60°$ to $70°$ E (Fig. 7) shows that the cold anomalies enter tropical latitudes at midlevels. This intrusion makes the lower atmosphere convectively unstable and the upper atmosphere stable. These cold anomalies descend downward as time progresses making the lower atmosphere highly unstable near the western branch of the monsoon trough. Consequently, we see active convection in this region (not shown).

The moisture supply for LEREs is observed mainly near the southern branch of monsoon trough (Please see Figure 3b of Nikumbh et al. (2020)). The strengthening of monsoon trough by CAH can in turn bring more moisture from the Arabian sea into central India at its southern branch. Nikumbh et al. (2020) show that the presence of SCV facilitate the deep layer moisture flux during LEREs. This moisture transport can be enhanced further by the monsoon trough circulation in the presence of extratropical forcing.

4. Summary and discussion

We observe tropical-extratropical interactions during LEREs over central India. A couplet of blocking high and low forms over the northeast Atlantic about a week before LEREs. This couplet is accompanied by a split jet as suggested by the earlier studies (Shutts 1983; Trenberth 1986; Haines and Marshall 1987). The ABH continues to amplify and strengthen the downstream disturbances forming a Rossby wave train (Fig. 8). The CAH that forms downstream along this train is amplified and it comes in phase with the monsoon trough at mid and low-levels. It strengthens the equatorial monsoon trough by providing momentum, dynamic forcing, and static instabilities. It also facilitates the Rossby wave breaking and transports high PV equatorward. A high PV intrusion is observed west to LEREs that can induce vertical motion and static instabilities leading to extreme convection. Here, we note that moisture for LEREs is supplied by tropical circulation associated with LPS and SCV, as suggested by Nikumbh et al. (2020) (their Figure 3b). Extratropical forcing supplies additional dynamic and thermodynamic forcing, and strengthens the monsoon trough in which synoptic-scale LPS and SCV are embedded. The location of CAH is such that it can directly interact with the western branch of the monsoon trough in which SCV is embedded (Fig. 6). We expect that extratropical interaction would result in the strengthening of
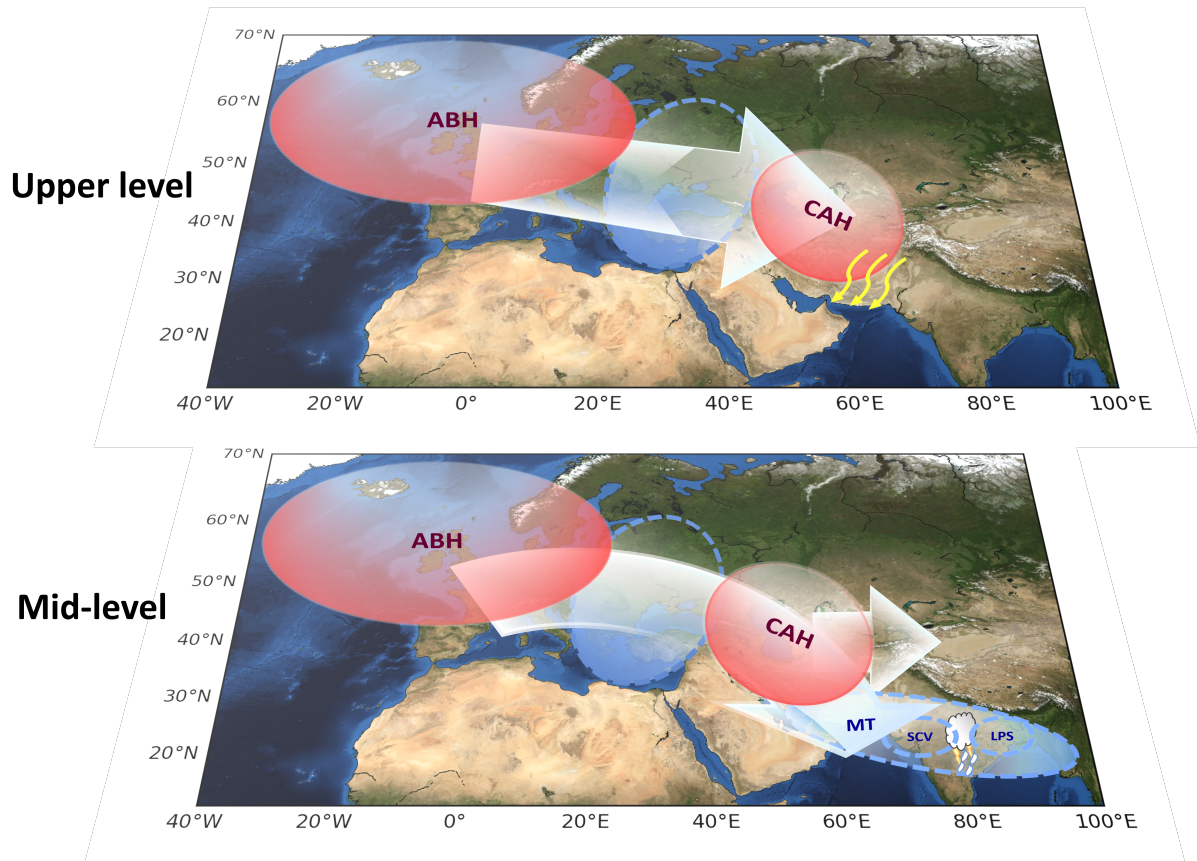
18

FIG. 8. Schematic explaining the tropical-extratropical interactions during large-scale extreme rainfall events (LEREs) over central India. The acronyms ABH, CAH, MT, SCV and LPS indicate Atlantic blocking high, central Asian high, equatorial monsoon trough, secondary cyclonic vortex and monsoon low-pressure system, respectively. Big white arrows represent the path of wave momentum transport. Yellow arrows represents the wave breaking faciliated by central Asian high that enables high potential vorticity transport equatorward. The monsoon trough is strengthened by extratropical forcing. LEREs are produced in between LPS and SCV, embedded in the equatorial monsoon trough.

SCV. A modeling study might help in quantifying the contribution from the extratropical forcing in intensifying monsoon trough, SCV, LPS and thereby during LEREs. Large-scale conditions such as the North Atlantic Oscillation (NAO), Atlantic Multidecadal Oscillation (AMO), El Niño–Southern Oscillation (ENSO) and Madden–Julian oscillation (MJO) are known to modulate the occurrence of ABH and the associated teleconnection pattern (Shabbar et al. 2001; Häkkinen et al. 2011; Henderson and Maloney 2018; Henderson et al. 2016). Further investigation of these factors might help understand the results reported in this study better.

19

Using the nonuniform basic state formulation of the Rossby wave ray tracing (Karoly 1983; Li et al. 2015), we show that the waves generated over the Atlantic ocean can come over India during the monsoon following a great circle path at midlevels. On the other hand, waves at upper level travel along the westerly jet, then recurve near east Asia ($100 - 120°$ E) and come over the Indian subcontinent. The underlying assumptions for the calculation of the ray path include (1) a stationary source, (2) smoothly varying background flow, and (3) no dissipation. The prevalent conditions in the real atmosphere are quite different from these ideal assumptions, so we do not expect the exact match between the path followed by the Rossby wave response observed during LEREs and the path presented in Section 3a. Nonetheless, the ray tracing exercise gives some qualitative insights into the Rossby wave propagation. We see that the extratropical Rossby waves can intrude at midlevels over northwest India. The geopotential height anomalies at 500 hPa during LEREs closely follow the great circle path starting from the west coast of Africa till the monsoon trough (Supplementary Figure 28). It is more clear especially since day(-4) when the disturbances over central Asia start strengthening. The stationary wave activity flux orginating from the Atlantic blocking high during LEREs also has a component that approximately follows the Rossy ray path (Figure 5). We see the CAH transports wave activity southward at 500 hPa that intrudes into the tropics (south of $30°$ N) and interacts with the monsoon trough (Figure 5). On the other hand, the wave activity flux at the upper level remains north of $30°$ N (Supplementary Figure 26). This suggests that tropical-extratropical interactions during the summer monsoon can occur over northwest India, mainly at mid levels and a possible pathway is a great circle route, as suggested by the ray tracing. We note that the meridional versus zonal propagation of waves at mid- and upper level is obtained here only using the background flow. However, the amount of a forcing can also determine the propagation of the waves (Lutsko and Held 2016).

The role of Atlantic blocking high on triggering weather extremes over European countries is well known (Sillmann and Croci-Maspoli 2009; Dole et al. 2011; Lenggenhager et al. 2019). Studies have highlighted the role of European blocking high in triggering 2010 Pakistan flood event (Hong et al. 2011) and a recent 2022 Pakistan flood (Hsu et al. 2022). Here, we see that it can have far reaching remote influences, in facilitating LEREs over central India. In previous studies, the influence of extratropical forcing during the summer monsoon has been investigated mainly for heavy rainfall events of the northern parts of the Indian subcontinent and Himalayan extremes

20

(Vellore et al. 2016; Lau and Kim 2012; Martius et al. 2013; Hunt et al. 2018; Priya et al. 2017; Bohlinger et al. 2017) or in the context of monsoon break events (Ramaswamy 1958, 1962; Raman and Rao 1981; Krishnan et al. 2009; Samanta et al. 2016; Borah et al. 2020). Here, we show that extratropical forcing play an important role even during the large-scale heavy rainfall events of central India.

Data availability statement. The rainfall data used in the study is obtained from the IMD (`https://www.imdpune.gov.in/Clim_Pred_LRF_New/Grided_Data_Download.html`). The reanalysis dataset is available at `https://www.ecmwf.int/en/forecasts/datasets/reanalysis-datasets/era-interim`.

References

Barriopedro, D., R. García-Herrera, A. R. Lupo, and E. Hernández, 2006: A climatology of northern hemisphere blocking. *Journal of climate*, **19 (6)**, 1042–1063.

Bjerknes, J., 1969: Atmospheric teleconnections from the equatorial pacific. *Monthly weather review*, **97 (3)**, 163–172.

Bluestein, H., 1992: Synoptic-dynamic meteorology in midlatitudes: Volume 1, principles of kinematics and dynamics. 197.

Bohlinger, P., A. Sorteberg, and H. Sodemann, 2017: Synoptic conditions and moisture sources actuating extreme precipitation in nepal. *Journal of Geophysical Research: Atmospheres*, **122 (23)**, 12–653.

Borah, P., V. Venugopal, J. Sukhatme, P. Muddebihal, and B. Goswami, 2020: Indian monsoon derailed by a north atlantic wavetrain. *Science*, **370 (6522)**, 1335–1338.

Branstator, G., 1983: Horizontal energy propagation in a barotropic atmosphere with meridional and zonal structure. *Journal of Atmospheric Sciences*, **40 (7)**, 1689–1708.

Chakraborty, A., 2016: A synoptic-scale perspective of heavy rainfall over chennai in november 2015. *Current Science (00113891)*, **111 (1)**.

Chakraborty, A., and S. Agrawal, 2017: Role of west asian surface pressure in summer monsoon onset over central india. *Environmental Research Letters*, **12 (7)**, 074 002.

Charney, J. G., 1969: A further note on large-scale motions in the tropics. *Journal of the Atmospheric Sciences*, **26 (1)**, 182–185.

Chen, T.-C., M.-C. Yen, W.-R. Huang, and W. A. Gallus Jr, 2002: An east asian cold surge: case study. *Monthly weather review*, **130 (9)**, 2271–2290.

Chen, T.-C., M.-C. Yen, J.-D. Tsay, N. T. Tan Thanh, and J. Alpert, 2012: Synoptic development of the hanoi heavy rainfall event of 30–31 october 2008: Multiple-scale processes. *Monthly weather review*, **140 (4)**, 1219–1240.

Cheng, X., and J. M. Wallace, 1993: Cluster analysis of the northern hemisphere wintertime 500-hpa height field: Spatial patterns. *Journal of atmospheric sciences*, **50 (16)**, 2674–2696.

De Vries, A. J., H. G. Ouwersloot, S. B. Feldstein, M. Riemer, A. M. El Kenawy, M. F. McCabe, and J. Lelieveld, 2018: Identification of tropical-extratropical interactions and extreme precipitation events in the middle east based on potential vorticity and moisture transport. *Journal of Geophysical Research: Atmospheres*, **123 (2)**, 861–881.

Dee, D. P., and Coauthors, 2011: The ERA-Interim reanalysis: configuration and performance of the data assimilation system. *Quarterly Journal of the Royal Meteorological Society*, **137 (656)**, 553–597.

Di Capua, G., M. Kretschmer, R. V. Donner, B. Van Den Hurk, R. Vellore, R. Krishnan, and D. Coumou, 2020: Tropical and mid-latitude teleconnections interacting with the indian summer monsoon rainfall: a theory-guided causal effect network approach. *Earth System Dynamics*, **11 (1)**, 17–34.

Ding, Q., and B. Wang, 2005: Circumglobal teleconnection in the northern hemisphere summer. *Journal of climate*, **18 (17)**, 3483–3505.

23

Ding, Q., and B. Wang, 2007: Intraseasonal teleconnection between the summer eurasian wave train and the indian monsoon. *Journal of Climate*, **20 (15)**, 3751–3767.

Ding, Q., and B. Wang, 2009: Predicting extreme phases of the indian summer monsoon. *Journal of Climate*, **22 (2)**, 346–363.

Dole, R., and Coauthors, 2011: Was there a basis for anticipating the 2010 russian heat wave? *Geophysical Research Letters*, **38 (6)**.

Falcão, A. X., J. Stolfi, and R. de Alencar Lotufo, 2004: The image foresting transform: Theory, algorithms, and applications. *IEEE transactions on pattern analysis and machine intelligence*, **26 (1)**, 19–29.

Feng, J., W. Chen, and Y. Li, 2017: Asymmetry of the winter extra-tropical teleconnections in the northern hemisphere associated with two types of enso. *Climate Dynamics*, **48 (7-8)**, 2135–2151.

Freitas, A. C. V., and V. B. Rao, 2014: Global changes in propagation of stationary waves in a warming scenario. *Quarterly Journal of the Royal Meteorological Society*, **140 (679)**, 364–383.

Funatsu, B. M., and D. W. Waugh, 2008: Connections between potential vorticity intrusions and convection in the eastern tropical pacific. *Journal of the Atmospheric Sciences*, **65 (3)**, 987–1002.

Haines, K., and J. Marshall, 1987: Eddy-forced coherent structures as a prototype of atmospheric blocking. *Quarterly Journal of the Royal Meteorological Society*, **113 (476)**, 681–704.

Häkkinen, S., P. B. Rhines, and D. L. Worthen, 2011: Atmospheric blocking and atlantic multi-decadal ocean variability. *Science*, **334 (6056)**, 655–659.

Henderson, S. A., and E. D. Maloney, 2018: The impact of the madden–julian oscillation on high-latitude winter blocking during el niño–southern oscillation events. *Journal of Climate*, **31 (13)**, 5293–5318.

Henderson, S. A., E. D. Maloney, and E. A. Barnes, 2016: The influence of the madden–julian oscillation on northern hemisphere winter blocking. *Journal of Climate*, **29 (12)**, 4597–4616.

Hong, C.-C., H.-H. Hsu, N.-H. Lin, and H. Chiu, 2011: Roles of european blocking and tropical-extratropical interaction in the 2010 pakistan flooding. *Geophysical Research Letters*, **38 (13)**.

24

Hoskins, B., 1997: A potential vorticity view of synoptic development. *Meteorological Applications: A journal of forecasting, practical applications, training techniques and modelling*, **4 (4)**, 325–334.

Hoskins, B., and P. Berrisford, 1988: A potential vorticity perspective of the storm of 15–16 october 1987. *Weather*, **43 (3)**, 122–129.

Hoskins, B., I. Draghici, and H. Davies, 1978: A new look at the ω-equation. *Quarterly Journal of the Royal Meteorological Society*, **104 (439)**, 31–38.

Hoskins, B., A. Simmons, and D. Andrews, 1977: Energy dispersion in a barotropic atmosphere. *Quarterly Journal of the Royal Meteorological Society*, **103 (438)**, 553–567.

Hoskins, B. J., and D. J. Karoly, 1981: The steady linear response of a spherical atmosphere to thermal and orographic forcing. *Journal of Atmospheric Sciences*, **38 (6)**, 1179–1196.

Hoskins, B. J., M. E. McIntyre, and A. W. Robertson, 1985: On the use and significance of isentropic potential vorticity maps. *Quarterly Journal of the Royal Meteorological Society*, **111 (470)**, 877–946.

Hsu, H., C. Hong, A. Huang, W. Tseng, M. Lu, and C. Chang, 2022: Linkage between record floods in pakistan and a severe heatwave in china in the boreal summer of 2022. URL https://doi.org/10.21203/rs.3.rs-2353452/v1.

Hunt, K. M., A. G. Turner, and L. C. Shaffrey, 2018: Extreme daily rainfall in pakistan and north india: Scale interactions, mechanisms, and precursors. *Monthly Weather Review*, **146 (4)**, 1005–1022.

Karoly, D. J., 1983: Rossby wave propagation in a barotropic atmosphere. *Dynamics of Atmospheres and Oceans*, **7 (2)**, 111–125.

Kiladis, G. N., 1998: Observations of rossby waves linked to convection over the eastern tropical pacific. *Journal of Atmospheric Sciences*, **55 (3)**, 321–339.

Kiladis, G. N., C. D. Thorncroft, and N. M. Hall, 2006: Three-dimensional structure and dynamics of african easterly waves. part i: Observations. *Journal of the atmospheric sciences*, **63 (9)**, 2212–2230.

25

Kiladis, G. N., and K. M. Weickmann, 1992: Extratropical forcing of tropical pacific convection during northern winter. *Monthly weather review*, **120 (9)**, 1924–1939.

Kimoto, M., and M. Ghil, 1993: Multiple flow regimes in the northern hemisphere winter. part i: Methodology and hemispheric regimes. *Journal of the Atmospheric Sciences*, **50 (16)**.

Knippertz, P., 2007: Tropical–extratropical interactions related to upper-level troughs at low latitudes. *Dynamics of Atmospheres and Oceans*, **43 (1-2)**, 36–62.

Kosaka, Y., J. Chowdary, S.-P. Xie, Y.-M. Min, and J.-Y. Lee, 2012: Limitations of seasonal predictability for summer climate over east asia and the northwestern pacific. *Journal of Climate*, **25 (21)**, 7574–7589.

Kripalani, R., A. Kulkarni, and S. Singh, 1997: Association of the indian summer monsoon with the northern hemisphere mid-latitude circulation. *International Journal of Climatology*, **17 (10)**, 1055–1067.

Krishnan, R., V. Kumar, M. Sugi, and J. Yoshimura, 2009: Internal feedbacks from monsoon–midlatitude interactions during droughts in the indian summer monsoon. *Journal of the Atmospheric Sciences*, **66 (3)**, 553–578.

Lau, W. K., and K.-M. Kim, 2012: The 2010 pakistan flood and russian heat wave: Teleconnection of hydrometeorological extremes. *Journal of Hydrometeorology*, **13 (1)**, 392–403.

Lenggenhager, S., M. Croci-Maspoli, S. Brönnimann, and O. Martius, 2019: On the dynamical coupling between atmospheric blocks and heavy precipitation events: A discussion of the southern alpine flood in october 2000. *Quarterly Journal of the Royal Meteorological Society*, **145 (719)**, 530–545.

Li, Y., J. Li, F. F. Jin, and S. Zhao, 2015: Interhemispheric propagation of stationary rossby waves in a horizontally nonuniform background flow. *Journal of the Atmospheric Sciences*, **72 (8)**, 3233–3256.

Lutsko, N. J., and I. M. Held, 2016: The response of an idealized atmosphere to orographic forcing: Zonal versus meridional propagation. *Journal of the Atmospheric Sciences*, **73 (9)**, 3701–3718.

26

Lyngwa, R. V., and M. A. Nayak, 2021: Atmospheric river linked to extreme rainfall events over kerala in august 2018. *Atmospheric Research*, **253**, 105 488.

Martius, O., and Coauthors, 2013: The role of upper-level dynamics and surface processes for the pakistan flood of july 2010. *Quarterly Journal of the Royal Meteorological Society*, **139 (676)**, 1780–1797.

Nakamura, H., M. Nakamura, and J. L. Anderson, 1997: The role of high-and low-frequency dynamics in blocking formation. *Monthly Weather Review*, **125 (9)**, 2074–2093.

Nakamura, N., and C. S. Huang, 2018: Atmospheric blocking as a traffic jam in the jet stream. *Science*, **361 (6397)**, 42–47.

Narinesingh, V., J. F. Booth, S. K. Clark, and Y. Ming, 2020: Atmospheric blocking in an aquaplanet and the impact of orography. *Weather and Climate Dynamics*, **1 (2)**, 293–311.

Nikumbh, A. C., A. Chakraborty, and G. Bhat, 2019: Recent spatial aggregation tendency of rainfall extremes over india. *Scientific reports*, **9 (1)**, 10 321.

Nikumbh, A. C., A. Chakraborty, G. Bhat, and D. M. Frierson, 2020: Large-scale extreme rainfall producing synoptic systems of the indian summer monsoon. *Geophysical Research Letters*, e2020GL088403.

Nikumbh, A. C., A. Chakraborty, G. S. Bhat, and D. M. W. Frierson, 2021: Multiscale interactions between monsoon intraseasonal oscillations and low pressure systems that produce heavy rainfall events of different spatial extents. *Journal of Climate*, **34 (23)**, 9523–9534.

Park, T.-W., C.-H. Ho, and Y. Deng, 2014: A synoptic and dynamical characterization of wave-train and blocking cold surge over east asia. *Climate dynamics*, **43 (3-4)**, 753–770.

Pelly, J. L., and B. J. Hoskins, 2003: A new perspective on blocking. *Journal of the atmospheric sciences*, **60 (5)**, 743–755.

Postel, G. A., and M. H. Hitchman, 1999: A climatology of rossby wave breaking along the subtropical tropopause. *Journal of the Atmospheric Sciences*, **56 (3)**, 359–373.

Priya, P., R. Krishnan, M. Mujumdar, and R. A. Houze, 2017: Changing monsoon and midlatitude circulation interactions over the western himalayas and possible links to occurrences of extreme precipitation. *Climate Dynamics*, **49 (7)**, 2351–2364.

Rajeevan, M., J. Bhate, J. Kale, and B. Lal, 2006: High resolution daily gridded rainfall data for the indian region: Analysis of break and active. *Current Science*, **91 (3)**, 296–306.

Raman, C., and Y. Rao, 1981: Blocking highs over asia and monsoon droughts over india. *Nature*, **289 (5795)**, 271–273.

Ramaswamy, C., 1958: A preliminary study of the behaviour of the indian southwest monsoon in relation to the westerly jet-stream. *Geophysica*, **6**, 455–476.

Ramaswamy, C., 1962: Breaks in the indian summer monsoon as a phenomenon of interaction between the easterly and the sub-tropical westerly jet streams. *Tellus*, **14 (3)**, 337–349.

Riehl, H., 1950: On the role of the tropics in the general circulation of the atmosphere. *Tellus*, **2 (1)**, 1–17.

Rondanelli, R., B. Hatchett, J. Rutllant, D. Bozkurt, and R. Garreaud, 2019: Strongest mjo on record triggers extreme atacama rainfall and warmth in antarctica. *Geophysical Research Letters*, **46 (6)**, 3482–3491.

Samanta, D., M. Dash, B. Goswami, and P. Pandey, 2016: Extratropical anticyclonic rossby wave breaking and indian summer monsoon failure. *Climate Dynamics*, **46 (5-6)**, 1547–1562.

Sanders, R., 1953: Blocking highs over the eastern north atlantic ocean and western europe. *Monthly Weather Review*, **81 (3)**, 67–73.

Sardeshmukh, P., 1987: A diagnostic study of the dynamics of the northern hemisphere winter of 1985–1986. *Quart. J. Roy. Meteor. Soc*, **113**, 759–778.

Shabbar, A., J. Huang, and K. Higuchi, 2001: The relationship between the wintertime north atlantic oscillation and blocking episodes in the north atlantic. *International journal of climatology*, **21 (3)**, 355–369.

Shutts, G., 1983: The propagation of eddies in diffluent jetstreams: Eddy vorticity forcing of 'blocking' flow fields. *Quarterly Journal of the Royal Meteorological Society*, **109 (462)**, 737–761.

Sillmann, J., and M. Croci-Maspoli, 2009: Present and future atmospheric blocking and its impact on european mean and extreme climate. *Geophysical Research Letters*, **36 (10)**.

Sooraj, K., P. Terray, A. Shilin, and M. Mujumdar, 2020: Dynamics of rainfall extremes over india: A new perspective. *International Journal of Climatology*, **40 (12)**, 5223–5245.

Stan, C., D. M. Straus, J. S. Frederiksen, H. Lin, E. D. Maloney, and C. Schumacher, 2017: Review of tropical-extratropical teleconnections on intraseasonal time scales. *Reviews of Geophysics*, **55 (4)**, 902–937.

Takaya, K., and H. Nakamura, 2001: A formulation of a phase-independent wave-activity flux for stationary and migratory quasigeostrophic eddies on a zonally varying basic flow. *Journal of Atmospheric Sciences*, **58 (6)**, 608–627.

Trenberth, K., 1986: The signature of a blocking episode on the general circulation in the southern hemisphere. *Journal of the atmospheric sciences*, **43 (19)**, 2061–2069.

Vanneste, J., and T. Shepherd, 1998: On the group-velocity property for wave-activity conservation laws. *Journal of the atmospheric sciences*, **55 (6)**, 1063–1068.

Vautard, R., 1990: Multiple weather regimes over the north atlantic: Analysis of precursors and successors. *Monthly weather review*, **118 (10)**, 2056–2081.

Vellore, R. K., and Coauthors, 2016: Monsoon-extratropical circulation interactions in himalayan extreme rainfall. *Climate Dynamics*, **46 (11)**, 3517–3546.

Wang, Y., K. Yamazaki, and Y. Fujiyoshi, 2007: The interaction between two separate propagations of rossby waves. *Monthly weather review*, **135 (10)**, 3521–3540.

Waugh, D. W., and B. M. Funatsu, 2003: Intrusions into the tropical upper troposphere: Three-dimensional structure and accompanying ozone and olr distributions. *Journal of the atmospheric sciences*, **60 (4)**, 637–653.

Waugh, D. W., and L. M. Polvani, 2000: Climatology of intrusions into the tropical upper troposphere. *Geophysical Research Letters*, **27 (23)**, 3857–3860.

Webster, P. J., and J. R. Holton, 1982: Cross-equatorial response to middle-latitude forcing in a zonally varying basic state. *Journal of Atmospheric Sciences*, **39 (4)**, 722–733.

Wernli, H., and M. Sprenger, 2007: Identification and era-15 climatology of potential vorticity streamers and cutoffs near the extratropical tropopause. *Journal of the atmospheric sciences*, **64 (5)**, 1569–1586.

Woollings, T., B. Hoskins, M. Blackburn, and P. Berrisford, 2008: A new rossby wave–breaking interpretation of the north atlantic oscillation. *Journal of the Atmospheric Sciences*, **65 (2)**, 609–626.

Zhao, S., J. Li, and Y. Li, 2015: Dynamics of an interhemispheric teleconnection across the critical latitude through a southerly duct during boreal winter. *Journal of Climate*, **28 (19)**, 7437–7456.